Modelling the spectral induced polarization response of water-saturated sands in the intermediate frequency range (102–105 Hz) using mechanistic and empirical approaches

Thomas Kremer, Myriam Schmutz, Philippe Leroy, Pierre Agrinier, Alexis Maineult

Geophysical Journal International

Geophys. J. Int. (2016) **207,** 1303–1312
Advance Access publication 2016 September 7
GJI Marine geosciences and applied geophysics

doi: 10.1093/gji/ggw334

Modelling the spectral induced polarization response of water-saturated sands in the intermediate frequency range (10^2–10^5 Hz) using mechanistic and empirical approaches

Thomas Kremer,[1,2] Myriam Schmutz,[3] Philippe Leroy,[4] Pierre Agrinier[1,2] and Alexis Maineult[1,2]

[1] *Institut de Physique du Globe de Paris, Sorbonne Paris Cité, Univ. Paris Diderot, F-*75005 *Paris, France. E-mail: alexis.maineult@upmc.fr*
[2] *Centre de Recherches sur le Stockage Géologique du CO_2 (IPGP/TOTAL/SCHLUMBERGER/ADEME), F-*75005 *Paris, France*
[3] *EA*4592 *- Bordeaux INP - ENSEGID, F-*33607 *Pessac, France*
[4] *BRGM, French Geological Survey, F-*45060 *Orléans, France*

Accepted 2016 September 2. Received 2016 September 2; in original form 2015 December 21

SUMMARY

The intermediate frequency range 10^2–10^5 Hz forms the transition range between the spectral induced polarization frequency domain and the dielectric spectroscopy frequency domain. Available experimental data showed that the spectral induced polarization response of sands fully saturated with water was particularly sensitive to variations of the saturating water electrical conductivity value in the intermediate frequency range. An empirical and a mechanistic model have been developed and confronted to this experimental data. This confrontation showed that the Maxwell Wagner polarization alone is not sufficient to explain the observed signal in the intermediate frequency range. The SIP response of the media was modelled by assigning relatively high dielectric permittivity values to the sand particle or high effective permittivity values to the media. Such high values are commonly observed in the dielectric spectroscopy literature when entering the intermediate frequency range. The physical origin of these high dielectric permittivity values is discussed (grain shape, electromagnetic coupling), and a preliminary study is presented which suggests that the high impedance values of the non-polarizable electrodes might play a significant role in the observed behaviour.

Key words: Electrical properties; Hydrogeophysics; Permeability and porosity.

1 INTRODUCTION

Electrical and electromagnetic geophysical methods aim at providing information relative to the structural and mineralogical characteristics of Earth materials, their fluid content and composition, and others soil properties in a non-intrusive way (Revil *et al*. 2012; Binley *et al*. 2015). Studying the nature, magnitude and dependence to frequency of the different polarization processes that can take place in the ground upon the application of an electrical field, is one of the strategies that can help retrieving this kind of information (Revil 2013).

Spectral induced polarization (SIP) method focus on studying the electrical properties of Earth materials generally in the low frequency range 10^{-3}–10^2 Hz, where interfacial polarization phenomena at the surface of the particles and inside metallic ones occur (e.g. Vinegar & Waxman 1984; Olhoeft 1985; De Lima & Sharma 1990). A detailed description of both theoretical and practical aspects associated with SIP method can be found in Chelidze & Guéguen (1999) and Chelidze *et al*. (1999). Researchers have developed models to describe the low frequency interfacial polarization processes and their magnitude, using an empirical approach (e.g. Weller *et al*. 2010), a semi-empirical approach (e.g. Cole & Cole 1941; Davidson & Cole 1951; Dias 2000), or a mechanistic approach (e.g. Leroy & Revil 2009; Jougnot *et al*. 2010; Bücker & Hördt 2013).

The dielectric spectroscopy method investigates the electrical properties of materials in the high frequency range (10^5–10^9 Hz). It has been widely used in geophysics (e.g. Taherian *et al*. 1990; Chelidze & Guéguen 1999; Lesmes & Morgan 2001) as well as in the medical field (e.g. Gabriel *et al*. 1996; Ishai *et al*. 2013). The polarization phenomenon occurring in this frequency range is known as the interfacial Maxwell–Wagner polarization. In geophysics, it results from the accumulation of charges at the interface between soil components that present different dielectric permittivity and electrical conductivity values. Models have been developed to describe the relaxation behaviour of Earth material in this frequency range. Some use an empirical approach (e.g. Topp & Reynolds 1998), some are based on the volume averaging method (Pride 1994) and others are based on the effective differential medium approach (e.g. Sen 1981; Mendelson & Cohen 1982; Cosenza *et al*. 2003).

As pointed out by Revil (2013), the relaxation behaviour of Earth materials has been much less studied in the intermediate frequency range (10^2–10^5 Hz), which constitutes the transition range between low frequency polarization and high frequency polarization. One of the main reasons for disregarding this part of the SIP spectra is because many parasitic effects can take place (e.g. electromagnetic coupling, electrode effects) which will mask the IP response of the studied media. However, the SIP signal in this frequency range is expected to provide valuable, complementary information compared to the low frequency range (e.g. Binley *et al*. 2005; Breede *et al*. 2012). Significant progress has been made in the acquisition of broadband SIP measurements in the laboratory and on the field (e.g. Zimmermann *et al*. 2008a; Radic 2014), and we observe an increasing interest for the study of this frequency range and of the parasitic effects associated (e.g. Abdulsamad *et al*. 2016; Huisman *et al*. 2016).

To describe the relaxation behaviour of Earth material in the intermediate frequency range, some authors have chosen to extend Maxwell–Wagner based model towards low frequencies (Chen & Or 2006) or to use the low frequency approach [polarization of the electrical double layer (EDL)] and to extend it to higher frequencies (Leroy *et al*. 2008). Revil (2013) also presented a unified model describing the SIP response of unsaturated sands over the whole frequency range (10^{-3}–10^9 Hz), which is remarkably precise in the lowest frequency domain ($f < 100$ Hz) but less in the intermediate frequency range (10^2–10^5 Hz). In this paper, we present the results of a modelling work which reproduces the intermediate frequency range SIP response of unconsolidated sands fully saturated with water. We investigated the dependence of the models parameters with the effective conductivity of the media, in this case mainly controlled by the electrical conductivity σ_w of the saturating water.

2 THEORETICAL BACKGROUND

2.1 SIP parameters

Four-electrodes SIP measurements in the laboratory consist of injecting in the studied sample a sinusoidal-shaped electrical signal of amplitude I through two electrodes, denoted A and B, and measuring the resulting voltage difference ΔV between another pair of electrodes denoted M and N. If polarization processes occur, a phase delay φ, expressed as an angle (in rad), is observed between the injected and the measured signal. From these parameters, one can calculate the effective complex conductivity σ^* given by:

$$\sigma^* = \left|\frac{I}{k\Delta V}\right| \exp(\mathrm{i}\varphi) = |\sigma| \exp(\mathrm{i}\varphi), \tag{1}$$

where i is the pure imaginary number and k is a geometric factor linked to the respective position of the four electrodes A, B, M and N, the size and shape of the sample, and the boundary conditions on the sample surface.

As a complex quantity, σ^* can be expressed in the quadratic form $\sigma^* = \sigma' + i\sigma''$. The real part σ' and the imaginary part σ'' of the complex conductivity, also respectively called the in-phase conductivity and the quadrature conductivity, are linked with the measured parameters by the relations $|\sigma| = (\sigma'^2 + \sigma''^2)^{1/2}$ and $\tan\varphi = \sigma'' / \sigma'$. The quadratic form of the complex conductivity is of particular interest in SIP studies because the in-phase conductivity σ' is mainly representative of the ohmic conduction properties of the medium, whereas the quadrature conductivity σ'' is mainly linked to the capacitive and inductive properties. The main objective of SIP measurements is to study the magnitude and the dependence to frequency of these parameters.

In practice, the quantity actually measured in SIP surveys is the effective complex conductivity σ^*_{eff} which links the total current density $\mathbf{J}_t$ going through the sample to the electrical field $\mathbf{E}$ through the relation (Revil 2013) $\mathbf{J}_t = \sigma^*_{\mathrm{eff}}\,\mathbf{E}$. This effective quantity takes in account the influence of the displacement current density $\mathbf{J}_d = \partial D/\partial t = \mathrm{i}\omega\varepsilon^*$ where ε^* is the complex permittivity that can be expressed as $\varepsilon^* = \varepsilon' + \mathrm{i}\varepsilon''$. The effective parameters that derive from $\sigma_{\mathrm{eff}}{}^*$ are the effective in-phase conductivity σ'_{eff} and the effective quadrature conductivity σ''_{eff}, respectively written as:

$$\begin{cases} \sigma'_{\mathrm{eff}} = \sigma' + \omega\varepsilon'' \\ \sigma''_{\mathrm{eff}} = \sigma'' + \omega\varepsilon' \end{cases}, \tag{2}$$

where σ', σ'', ε' and ε'' are frequency dependent scalars, positively defined. It is common in SIP surveys not to take in account the terms related to the sample complex permittivity ($\omega\varepsilon''$ and $\omega\varepsilon'$ in eq. 2), because they are generally negligible when the frequency is below 10 Hz ($\omega\varepsilon' \ll \sigma''$ and $\omega\varepsilon'' \ll \sigma'$). However, in this paper we focused on the intermediate frequency range 10^2–10^5 Hz response, which can be considered as elevated frequencies compared to the range classically investigated in SIP surveys, which is why in the following we use the effective parameters defined above.

2.2 Grain polarization model

2.2.1 Electro-chemical polarization of the EDL

The SIP model developed by Leroy *et al*. (2008) uses a mechanistic approach to describe the electro-chemical polarization of an isolating spherical silica grain, coated by a conductive electrical double layer. In their model, the compact Stern layer at the close proximity of the particle surface polarizes whereas the diffuse layer located further away from the surface is assumed to form a dielectric continuum that does not polarize.

Leroy *et al*. (2008) express the complex conductivity of such a particle as:

$$\sigma^*_s = \sigma_s + \mathrm{i}\omega\varepsilon_s, \tag{3}$$

where σ_s is the electrical conductivity of the particle coated by a conductive layer (S m^{-1}) and ε_s denotes its dielectric permittivity (F m^{-1}).

The electrical conductivity of the particle σ_s can be expressed as a function of the low frequency specific surface conductivity of the particle ${\Sigma_s}^0$ (in S, which corresponds to the conduction process in the diffuse layer) and the high frequency contribution of the Stern layer ${\Sigma_s}^\infty$:

$$\begin{cases} \sigma_s = \dfrac{2}{a_0}\left({\Sigma_s}^0 + {\Sigma_s}^\infty\right) - \dfrac{2}{a_0}\dfrac{{\Sigma_s}^\infty}{1 + \mathrm{i}\omega\tau_0} \\ \tau_0 = \dfrac{{a_0}^2}{2D_s} \end{cases}, \tag{4}$$

where a_0 is the silica particle radius (m) and τ_0 the relaxation time (s) associated with the particle size and the diffusion coefficient of the counter-ions in the Stern layer D_s (in m^{2}s^{-1}). Parameters ${\Sigma_s}^0$ and ${\Sigma_s}^\infty$ are related to the electrochemical properties of the media:

$$\begin{cases} {\Sigma_s}^0 = e{\beta_{\mathrm{Na}+}}^d\,{\Gamma_{\mathrm{Na}+}}^d + {\Sigma_s}^0\left(\mathrm{H}^+\right) \\ {\Sigma_s}^\infty = e{\beta_{\mathrm{Na}+}}^s\,{\Gamma_{\mathrm{Na}+}}^{s,0} \end{cases}, \tag{5}$$

where ${\beta_{\mathrm{Na}+}}^s$ is the ionic mobility of Na^+ ions in the Stern layer (m^{2}s^{-1}V^{-1}), ${\beta_{\mathrm{Na}+}}^d$ the ionic mobility in the diffuse layer, e the

electronic charge ($e = 1.602 \times 10^{-19}$ C), $\Gamma_{Na+}{}^{d}$ the surface density of the counter-ions Na^+ adsorbed in the diffuse layer (m^{-2}), $\Gamma_{Na+}{}^{s,0}$ the surface density of the counter-ions in the Stern layer (m^{-2}) and $\Sigma_s{}^0(H^+)$ the contribution to surface conductivity of the protons adsorbed on the particle surface ($S\,m^{-1}$).

Using eqs (2)–(5), one can calculate the complex conductivity of a single spherical particle whose radius is a_0. In the case of a granular medium characterized by a distribution of grain radii, the effective complex conductivity of the medium can be calculated using the convolution product between the grain size distribution function $f(a)$ and the complex conductivity of a single particle of radius a:

$$\sigma_{\text{eff}}{}^{*} = f(a) \otimes \sigma_s{}^{*}(a, \omega). \tag{6}$$

In our case, we used the grain size distribution function of the Cole–Cole form (Cole & Cole 1941), which was successfully used by Vaudelet *et al*. (2011) to model the SIP response of similar sands:

$$f(a) = \frac{1}{2\pi a} \frac{\sin(\pi(1-\alpha))}{\cosh\left(2\alpha \ln \frac{a}{a_{\text{ave}}}\right) - \cos(\pi(1-\alpha))}, \tag{7}$$

where a_{ave} is the average radius of the particle distribution (m) and α is the Cole–Cole exponent ($0 < \alpha < 1$).

2.2.2 *Maxwell–Wagner polarization*

In our spectral induced polarization experiment, the porous sample is constituted of a solid and a liquid phase, that is of sand grains and surrounding water that have different dielectric permittivity and electrical conductivity values. Maxwell–Wagner polarization is caused by the formation of field-induced free charge distributions near the interface between the different phases (Maxwell 1892; Wagner 1914) and usually occurs in the intermediate frequency range (10^2–10^5 Hz) (Revil 2013).

Permittivity or conductivity models based on the differential effective medium (DEM) theory have successfully modelled the Maxwell–Wagner polarization of porous materials (Bruggeman 1935; Hanai 1968; Sen 1981). In the DEM theory, solid particles are embedded in a self-similar or self-consistent way in the pore water. First, a particle is added to the liquid and the influence of the particle upon the conductivity of the medium is calculated. Then, the particle/liquid mixture is used to coat a second particle and the influence of the second particle upon the conductivity of the medium is calculated, and so on following an iterative procedure until the desired porosity is reached. The DEM theory assumes that the pore space of granular media is interconnected. It works well to describe the electrical properties of uncompacted and uncemented granular media with small contiguity between the grains (Revil 2000).

The DEM theory is used for the calculation of the complex electrical conductivity of the water saturated sands $\sigma_n{}^{*}$ (i.e. of the sand grains and of their pore water). The initial electrical conductivity of the water saturated sands is the electrical conductivity of their pore water σ_{w}^{*}, that is $\sigma_n^{*} = \sigma_{\text{w}}^{*}$ ($\sigma_{\text{w}}^{*} = \sigma_{\text{w}} + i\omega\varepsilon_{\text{w}}$) with σ_{w} the bulk water conductivity and ε_{w} the bulk water permittivity). Inclusions are sand particles of surface conductivity $\sigma_s{}^{*}$ (including the effect of the particle size distribution on the surface conductivity) and infinitesimal volume fraction $\delta\Omega_n$. The complex conductivity of the water saturated sands is calculated iteratively using a Matlab procedure and the following equations:

$$L = 3 + \frac{\sqrt{9 - 60m + 36m^2}}{6m} \tag{8}$$

$$\delta\sigma_n^{*} = \frac{\sigma_n^{*}}{3} \frac{\delta\Omega_n}{1-\Omega_n} \times \frac{(\sigma_s^{*} - \sigma_n^{*})((1+3L)\sigma_s^{*} + (5-3L)\sigma_n^{*})}{(L\sigma_s^{*} + (1-L)\sigma_n^{*})((1-L)\sigma_s^{*} + (1+L)\sigma_n^{*})} \tag{9}$$

$$\sigma_n^{*} \text{ updated to } \sigma_n^{*} + \delta\sigma_n^{*} \tag{10}$$

$$\Omega_n \text{ updated to } \Omega_n + \delta\Omega_n, \tag{11}$$

where L is the depolarization coefficient of inclusions, which is calculated according to the value of the cementation exponent m (Mendelson & Cohen 1982). In eqs (9) and (11), the initial volume fraction of sand grains is equal to zero and the final volume fraction of inclusions is equal to $1 - \phi$ (ϕ is the porosity of the sample). The cementation exponent m enters into the first Archie's law $F = \phi^{-m}$. For spherical particles, $m = 1.5$ (Sen 1981) and for most granular media, $m = 2$ (Revil 2000). Eq. (8) can only be used if $m \geq 1.5$. If the porous medium is only constituted of pore water of complex conductivity σ_{w}^{*} or of sand grains of complex surface conductivity σ_s^{*}, the use of eqs (9)–(11) leads to $\sigma_n{}^{*} = \sigma_{\text{w}}^{*}$ and $\sigma_n{}^{*} = \sigma_s{}^{*}$, respectively. Furthermore, in the particular case of $m = 1.5$, according to eqs (8) and (9), we recover equation (78) of Leroy *et al*. (2008) ($L = 3$)

$$\delta\sigma_n^{*} = 3\sigma_n^{*} \frac{\sigma_s^{*} - \sigma_n^{*}}{2\sigma_n^{*} + \sigma_s^{*}} \delta\Omega_n. \tag{12}$$

3 MATERIALS AND METHOD

3.1 Experimental protocol

The modelling work presented in this paper is based on an attempt to reproduce some experimental data that was acquired during a laboratory scale experimental campaign (see Kremer *et al*. 2016). In particular, we will here focus on modelling the SIP response of unconsolidated granular media fully saturated with water of different electrical conductivity (EC) values (σ_{w} equal to 15, 40 and 100 mS m^{-1}, respectively, NaCl electrolyte). In every case, the saturating water pH value ranged between 8 and 8.8. Two types of sand were studied. A siliceous sand composed of 98 per cent mass of silica and 2 per cent mass of feldspars and micas, and a carbonated sand whose molar composition is 98 per cent calcium carbonate ($CaCO_3$) and 2 per cent magnesium carbonate ($MgCO_3$). Table 1 summarizes the grain size distribution and hydraulic properties of both sands (measured using a macropermeameter device whose functioning is fully described in Clavaud 2001).

Measurements were performed using a 40-cm-high, 30-cm-diameter cylindrical tank made of polyvinylchoride (PVC). The tank filling procedure consisted of building successive 3-cm-thick sand layers directly into the saturating water to ensure total saturation of the pore space, and applying manual compaction on the sand each time a layer is created. The relatively narrow grain size distribution of the sand ensures that the effects linked to layering or

Table 1. Summary of the grain size range and the hydraulic properties of the sands studied during the laboratory experimental campaign.

Sand type	Grain size range (μm)	Porosity	Permeability to water (D)
Silica	100–250	0.42	12.1 ± 0.3
Carbonated	50–400	0.32	4.0 ± 0.33

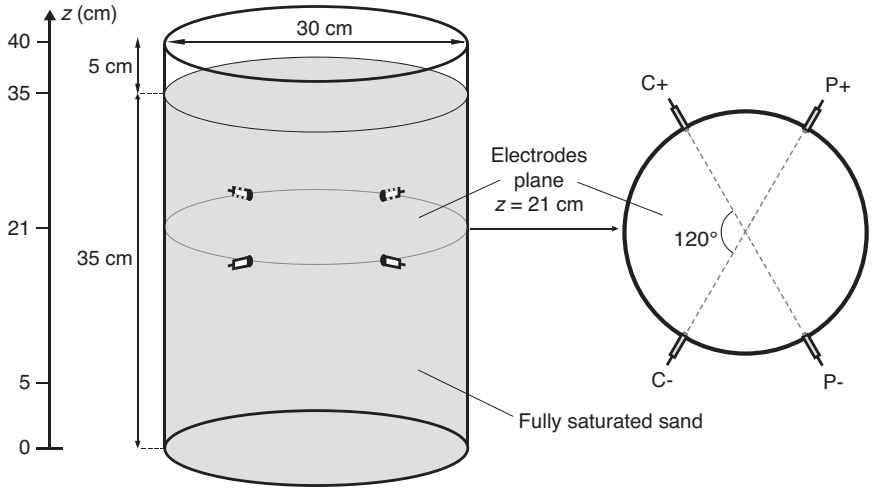

Figure 1. Sketch of the experimental set-up used to perform the measurements. Electrodes are set-up around the cylindrical tank at the height $z = 21$ cm. The sketch on the right shows a view from above of the electrode configuration used.

sorting of grains of different size are weak (Bairlein *et al*. 2014). The tank was filled up to a height $z = 35$ cm and the 4 electrodes were set-up around the tank in threaded holes following the display illustrated on Fig. 1. We privileged a 4 electrodes set-up rather than a 2 electrodes set-up in order to minimize electrode transfers or contact impedance effects (Chelidze *et al*. 1999; Volkmann & Klitzsch 2015). The specific position of the electrodes around the tank was chosen after performing a numerical sensitivity study with the forward modelling software R3t (Binley 2015). This configuration was a good compromise between homogeneity of the sensitivity distribution and elevated sensitivity values. The geometric factor value associated with the electrodes position and the height of the sand column was computed using the software R3t and was corroborated by measurements performed on water of known EC value. All measurements were performed using a SIP FUCHS III device (Radic 2004). The SIP parameters were investigated over the frequency range 0.5 Hz–20 kHz. Shielded coaxial cables were used for electrical potential measurements to limit as much as possible electromagnetic inductive coupling between the injection cables, measuring cables and the studied media. $Cu/CuSO_4$ non-polarizable electrodes were used for both current injection and potential measurements. Electrodes were tested for stability and ability to inject electrical current and measure electrical potential differences. A detailed description of all the tests conducted is given in Kremer *et al*. (2016). In particular, successive measurements were performed during 5 hr on the same kind of media than those studied during the experiments (silica sand fully saturated with water whose EC is 40 mS m^{-1}). The results demonstrated good measurement repeatability on the whole frequency range. The resistivity and the phase values variations were respectively less than 0.5 Ohm.m and 0.2 mrad. Hence, any signal variation stronger than this repeatability interval can safely be attributed to physico-chemical parameters.

In this study, our objective is to assess whether the experimental data acquired during this study can be reproduced by an empirical or a physicochemical model, focusing particularly on the intermediate frequency range.

3.2 Experimental results

During this experimental campaign, we mainly investigated the influence of the saturating water EC value σ_w upon the SIP response of these sands. Full details about how the experiences were conducted and how the conclusions were reached are given in Kremer *et al*. (2016). In the end, three main observations were made.

(1) The effective quadrature conductivity σ''_{eff}, linked to the capacitive properties and to the inductive response of the studied media, was systematically more affected by σ_w value variations when the frequency of the injected signal was in the intermediate frequency range 10^2–10^5 Hz. This point is illustrated on Fig. 2. For lower frequencies (1–10^2 Hz), variations could sometimes be observed but had a much weaker magnitude.

(2) In the intermediate frequency range 10^2–10^5 Hz, the magnitude of the effective quadrature conductivity σ''_{eff} increased with σ_w.

(3) Thirdly, we showed that the relative variations of the effective quadrature conductivity σ''_{eff} were always larger than the variations of bulk conductivity, classically measured in resistivity surveys, hence demonstrating the interest of the additional information brought by SIP method over classical resistivity methods.

These observations set the bases to justify a deeper investigation of the nature, the origin and the magnitude of the polarization processes that take place in the intermediate frequency range. To do so, we developed and applied an empirical and a mechanistic model to this set of data, in order to reproduce σ''_{eff} dependence with σ_w and studying which parameters control the intermediate frequency response of the systems studied.

4 EMPIRICAL MODELLING

Using the data presented on Fig. 2, we developed an empirical model that manages to reproduce the dependence of σ''_{eff} with the fluid EC value, in the range 10 Hz–20 kHz. To do so, we used the definition of the effective quadrature conductivity σ''_{eff} that was given earlier in Section 2.1: $\sigma''_{eff} = \sigma'' + \omega\varepsilon'$.

In theory, parameters σ'' and ε' values depend on ω (e.g. Sen & Chew 1983). In our empirical model, we consider them as non-frequency dependent, at least in the frequency range 10 Hz–20 kHz. With this hypothesis, the effective quadrature conductivity is defined by an affine linear relationship whose coefficients are respectively ε' and σ''. We used affine functions to fit the observed spectra in the intermediate frequency range (10 Hz–20 kHz) and obtained

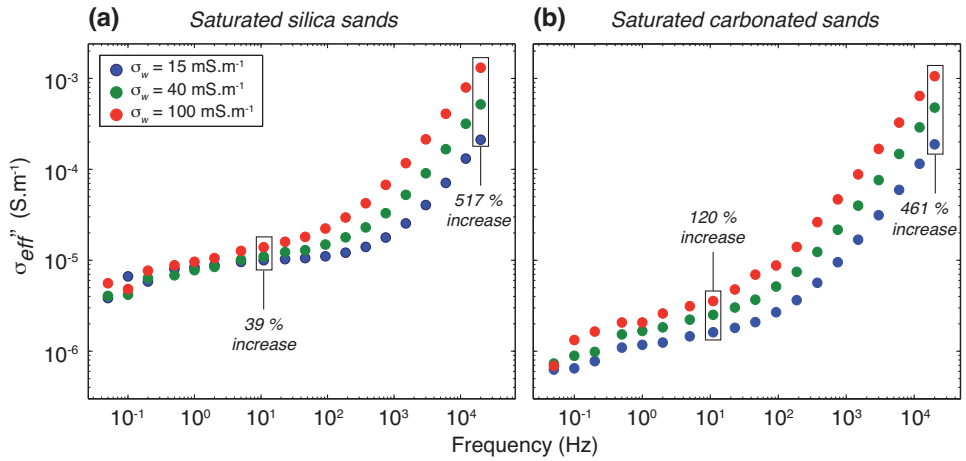

Figure 2. Spectra of the effective quadrature conductivity σ''_{eff} measured on silica sand (a) and carbonated sand (b) fully saturated with water of conductivity σ_{w}. For both sands, σ''_{eff} values increase with σ_{w} and relative variations are stronger in the intermediate frequency range 10^2–10^5 Hz than in the low frequency range ($f < 100$ Hz). The percentages on each graph indicate the relative variation of σ''_{eff} when σ_{w} value changes from 15 to 100 mS m^{-1}, at two specific frequencies (10 Hz and 20 kHz).

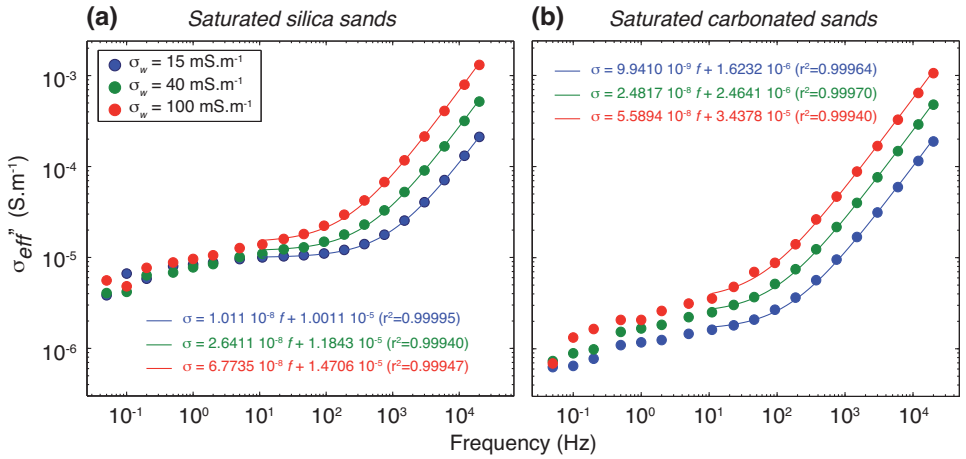

Figure 3. Fit of the effective quadrature conductivity in the intermediate frequency range ($f > 10$ Hz) of silica sand (a) and carbonated sand (b) fully saturated with water of varying electrical conductivity. Excellent regression coefficients are obtained using affine functions.

excellent regression coefficient values (adjustment coefficient $r^2 > 0.99$ on 12 points, Fig. 3). These results show that a simple linear model can indeed describe σ''_{eff} relation with frequency in the intermediate frequency range.

From ε' value, one can calculate the modelled relative permittivity value ε_r:

$$\varepsilon_r = \frac{\varepsilon'}{\varepsilon_0}, \tag{13}$$

where ε_0 is the dielectric permittivity of the vacuum ($\varepsilon_0 = 8.854\ 10^{-12}$ F m^{-1}).

Table 2 summarizes the different values of σ'' and ε_r obtained for each value of the saturating water EC, and for each sand type studied, using the affine empirical modelling previously described.

The most noteworthy feature of this study is that the relative permittivity values obtained to fit the data are very high compared to classical permittivity values of saturated sands (e.g. Knight & Nur 1987; West *et al.* 2003), and seem to increase with the EC value of the saturating water.

Table 2. Quadrature conductivity and relative permittivity values obtained by linearly fitting the intermediate frequency range ($f > 10$ Hz) experimental SIP results on each sand, for each water EC value.

	Silica sand		Carbonated sand	
σ_{w} (mS m^{-1})	σ'' (S m^{-1})	ε_r	σ'' (S m^{-1})	ε_r
15	1.00×10^{-5}	181	1.62×10^{-6}	179
40	1.18×10^{-5}	474	2.46×10^{-6}	446
100	1.47×10^{-5}	1217	3.44×10^{-6}	1005

5 MECHANISTIC MODELLING

In this section, we present the different steps that led to the fitting of our experimental data with the grain polarization model of the Stern layer from Leroy *et al.* (2008), which was described in Section 2. To expose properly the different steps taken, we first only consider the effective quadrature conductivity spectra obtained on silica sand fully saturated with water whose EC value is 15 mS m^{-1}.

Fig. 4(a) shows the experimental spectra and the grain polarization model result obtained by using parameters values extracted from the literature. We call this the 'literature based' model. Line 1 from Table 3 summarizes the values of the TLM parameters, and

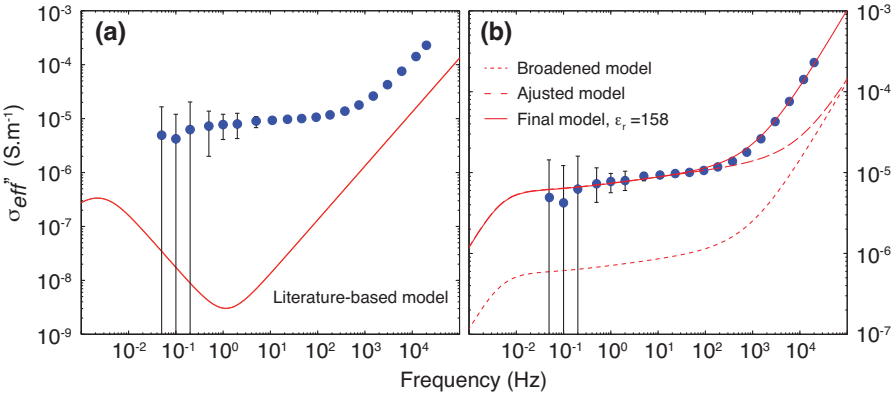

Figure 4. Representation of the four steps leading to the fitting of the TLM model with the experimental data acquired on silica sand fully saturated with water at 15 mS m^{-1}. (a) Using realistic parameters from the literature; (b) after broadening the relaxation time distribution; (c) after increasing the surface charge density in the Stern and in the diffuse layer; (d) after increasing the relative dielectric permittivity value of the sand particles.

Table 3. Evolution of the TLM model parameters during the different steps leading to the fitting of the experimental data presented in Fig. 4 (silica sand saturated with water whose EC equal to 15 mS m^{-1}). (*) indicates values taken from Leroy *et al.* (2008). Bold numbers indicate parameters whose value has been modified compared to the 'literature-based' model.

	a_{min} (μm)	a_{max} (μm)	α	$\Gamma_{Na+}{}^{s,0}$ (m^{-2})	$\Gamma_{Na+}{}^{d}$ (m^{-2})	ε_{rs}
Literature-based model	100	250	0.5	5.5×10^{16} (*)	3×10^{16} (*)	4
Broadened model	**0.01**	250	**0.92**	5.5×10^{16} (*)	3×10^{16} (*)	4
Adjusted model	**0.01**	250	**0.92**	$\mathbf{55 \times 10^{16}}$	3×10^{16} (*)	4
Final model	**0.01**	250	**0.92**	$\mathbf{55 \times 10^{16}}$	3×10^{16} (*)	**158**

the published studies from which they were chosen. Ionic mobility values are taken from Vaudelet *et al.* (2011) and Revil & Glover (1998), who worked on the low frequency SIP response of similar silica sands. The counter-ions densities are taken from Leroy *et al.* (2008) who studied spherical silica beads, in the same pH range but in a different EC range than our experimental study. The grain size distribution corresponds to the real case (determined through sieving operations). The initial value of $\varepsilon_s = 4$ (see eq. 3) corresponds to the relative dielectric permittivity of amorphous silica (Sze & Ng 2006).

When using parameters values from published studies, the model output curve does not present the same shape as the experimental data (Fig. 4a). No plateau is observed for the lowest frequency range, but rather a relaxation peak centered on a frequency around the mHz range.

To obtain a plateau shape in the lowest frequency range, we broadened the range of relaxation times which can be achieved by enlarging the grain size distribution (see Table 3, line 2). The result of such modification is shown by the dotted line in Fig. 4(b). We call these parameters setting the 'broadened' model. The shape obtained is much more similar to the experimental spectra, but values are too low.

To adjust the model in terms of magnitude, we modified the counter-ions density values in the Stern layer $\Gamma_{Na+}{}^{s,0}$ to one order magnitude higher (see line 3 from Table 3). By doing so, we manage to fit the low frequency part of the model curve with the experimental data (dashed line in Fig. 4b).

At this point, only the intermediate frequency range part of the data is not correctly reproduced. It can be adjusted by modifying the dielectric permittivity value of the sand particle (ε_s in eq. 3). By manually fitting the model with experimental data, we obtained very similar values than for the empirical model presented in Section 3 (continuous line in Fig. 4b). The resulting model curves for each type of sand and each σ_w value are shown in Fig. 5. With this parameter setting (which implies a very flexible model), the data is reproduced remarkably well.

6 DISCUSSION

6.1 Low frequency model calibration

The way that we calibrated the model parameters cannot always be justified physically. In the case of the broadening of the grain size distribution to obtain a wider relaxation times distribution, some authors who faced the same problem in their modelling work proposed as a physical justification the existence of non-linear interactions between the dipolar moments of each grain (Vaudelet *et al.* 2011). De Lima & Sharma (1990) suggest that the influence of membrane polarization phenomenon (polarization over multiple grain lengths) can be responsible for a widening of the relaxation time distribution. Lesmes & Morgan (2001) and Leroy *et al.* (2008) considered that the roughness of the grains increases the broadness of the modelled grain size distribution.

The counter-ions density values in the Stern layer $\Gamma_{Na+}{}^{s,0}$ used to calibrate the model for silica sands are one order of magnitude larger than the values found in Leroy *et al.* (2008). Those authors modelled the SIP response of silica beads in the same pH range but for lower ionic strength values (lower water EC). Therefore, the order of magnitude obtained here remains realistic since in this range of water EC values ($\sigma_w < 1$ S m^{-1}), the surface charge density is supposed to increase with the saturating water EC value (e.g. Lesmes & Frye 2001). In addition, Leroy *et al.* (2013) performed another modelling work on the SIP response of amorphous silica (Degussa) and found density values very close to those presented here in the same electrolytic conditions ([NaCl] ≈ 0.1 M and pH ≈ 8).

For the experiments involving carbonated sand, the counter-ions density values obtained with the grain polarization model are one

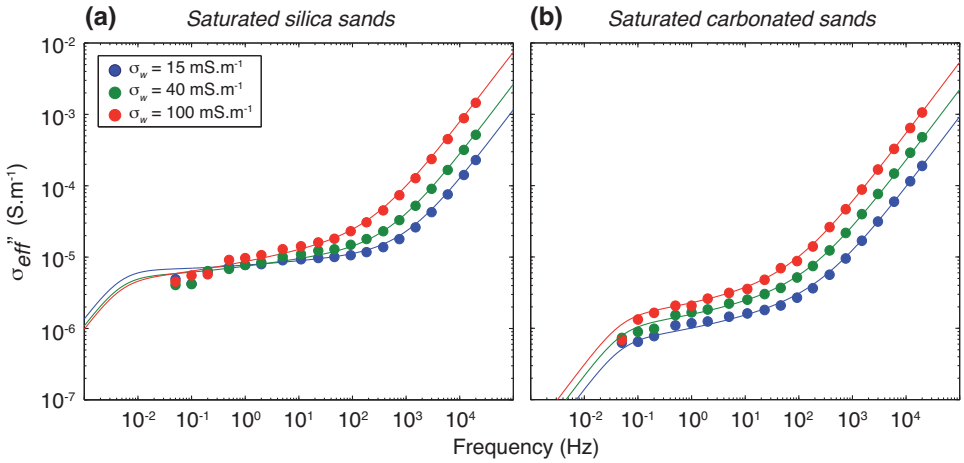

Figure 5. Fit of the effective quadrature conductivity with the TLM model, for the silica sand (a) and the carbonated (sand), at different water conductivities.

Table 4. Summary of the TLM parameters values obtained after fitting the experimental data obtained with each type of sand and each water EC value (see Fig. 5).

Sand type	σ_w (mS m^{-1})	α	$\Gamma_{Na+}^{s,0}$ (m^{-2})	ε_{rs}
Silica	15	0.92	5.5×10^{17}	158
Silica	40	0.87	4.6×10^{17}	384
Silica	100	0.82	4.5×10^{17}	1151
Carbonate	15	0.82	1.6×10^{16}	165
Carbonate	40	0.82	2.0×10^{16}	475
Carbonate	100	0.82	2.4×10^{16}	1090

order of magnitude lower than those obtained for silica sand (see Table 4). Although few published studies have explored the SIP response of carbonates materials, this difference is consistent with the study from Wu *et al*. (2009), who observed that calcite precipitation generally acts as a coating phase that can strongly inhibits the SIP response from granular media. Other corroborating arguments can be found in Guichet *et al*. (2006), who observed that the zeta potential of silica sands was significantly reduced when a calcite mineral phase had precipitated at the grain surface.

6.2 Intermediate frequency model calibration

6.2.1 Accordance with published studies

The intermediate frequency response (10^2 Hz $< f < 10^5$ Hz) of the systems studied has been fitted by assigning effective relative dielectric permittivity values (or particle dielectric permittivity value) in the order of 10^2 or 10^3 depending on the EC value of the saturating fluid. These values can seem relatively high compared to what can be observed in the high frequency range ($f > 10^5$ Hz) in dielectric spectroscopy studies performed on similar media, where values are generally in an order of magnitude about 10 (e.g. Knight & Nur 1987; West *et al*. 2003). However, many authors observe a significant increase of relative permittivity values towards the intermediate frequency range (e.g. Chew & Sen 1982; Kenyon 1984; Chen & Or 2006; Arcone & Boitnott 2012). Studies from Garrouch & Sharma (1994) and Lesmes & Morgan (2001) both report effective relative permittivity values of Berea sandstones ranging between 10^3 and 10^4 at a frequency of 10 kHz. Also, measured values are reported particularly high when the studied samples are fully saturated with water (e.g. Sengwa & Soni 2006; Gomaa 2008), which was the case in our experiments.

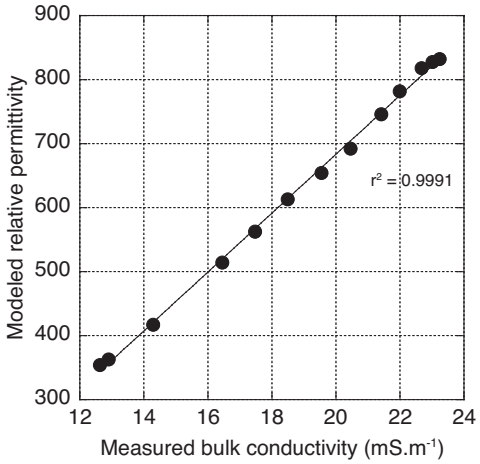

Figure 6. Linear relationship existing between the bulk conductivity of sand fully saturated with water and the relative permittivity values obtained by fitting the experimental data with the TLM model.

Also, the relative effective permittivity values (or particle permittivity values) obtained with the empirical and the grain polarization models (Tables 3 and 4) are clearly increasing with the EC value of the saturating fluid. Such tendency is in accordance with many published work (e.g. Sen 1981; Garrouch & Sharma 1994; Lasne *et al*. 2008). Study from Hilhorst (2000), later corroborated by Persson (2002), emphasize the existence of a linear relationship between the relative effective dielectric permittivity and the bulk conductivity of the media. Fig. 6 shows the relative permittivity values obtained by applying our model on a set of measurements performed on silica sands saturated with water whose EC value is progressively increased. A linear trend is clearly observed in the bulk conductivity range investigated, yielding an adjustment coefficient larger than 0.99 for 13 points.

6.2.2 Origin of the high dielectric permittivity values

6.2.2.1 Maxwell–Wagner polarization. The intermediate frequency behaviour of saturated Earth materials is generally attributed to the Maxwell–Wagner (MW) polarization (e.g. Chen & Or 2006). It results from charge accumulation at the interface between the soil's components that have different dielectric permittivity and

electric conductivity values. Chen & Or (2006) report that the dielectric permittivity values of the media are increasing with increasing fluid conductivity, which is in agreement with our experimental observations and with the behaviour of the model from Leroy *et al*. (2008).

However, even though MW polarization is taken in account in the grain polarization model from Leroy *et al*. (2008), we saw that it was not sufficient to match the experimental data in terms of magnitude. We managed to fit the data by considering the model very flexible, and by increasing significantly the relative effective permittivity of the media (in the empirical model) or of the particle (in the grain polarization model). This suggests that the Maxwell–Wagner effect alone cannot explain the measurements in the intermediate frequency range, and that other leads need to be discussed and investigated.

6.2.2.2 Influence of the grain shape. The dispersion behaviour of the Earth materials dielectric permittivity in the intermediate frequency range has been observed for a long time (e.g. Smith-Rose 1934; Keller & Licastro 1959; Howell & Licastro 1961). At that time, researchers mainly invoked instrumental effects related to the polarization of electrodes when approaching the intermediate frequency range and lower. However, even after attempting to correct experimental data from electrode polarization effects, Scott *et al*. (1967) still measure relative permittivity values in the order of 2000 on fully saturated rocks, at a frequency of 1 kHz.

Since then, many authors attribute this low frequency dispersion behaviour to geometric factors related to the shape of the grains composing the media. Sen (1981) demonstrates analytically that the presence of thin particles, even in weak concentrations, can lead to the increase of permittivity values. Jones & Friedman (2000) explore the same issue, focusing on the influence of the particle orientation on the measured permittivity values. Through a modelling work implying the moment method (see Tabbagh *et al*. 2002; Cosenza & Tabbagh 2004; Tabbagh *et al*. 2009) showed that the presence of thin particles such as clay sheets can give rise to particularly high effective dielectric permittivity values. It is therefore possible that the non-perfectly spherical shape of the grains composing the silica and carbonated sand is at least partly responsible for the high effective permittivity values observed. As an example supporting this hypothesis, Tabbagh *et al*. (2009) proposed an approximate regression law to compute the effective permittivity value ε_{eff} of a set of platelets, taking in account the effect of coupling between the cells:

$$\varepsilon_{\text{eff}} = \left(1 + 0.015\, C_t \frac{c}{e}\right) \varepsilon_r, \tag{14}$$

where C_t is the volumetric content of polarizable cells (in %), c/e is the flatness coefficient (side length over thickness, see Tabbagh *et al*. 2009), and ε_r is the relative molecular bulk permittivity. Considering a medium composed of 100 per cent of polarizable cells ($C_t = 100$), with very low flatness coefficient ($c/e = 1.5$), and to which we attribute a relative bulk permittivity value of 30 (dielectric constant of saturated sands, taken from Hubbard *et al*. 1997), we reach effective permittivity values in the order of 100, which is similar to what we obtain with the empirical model.

6.2.2.3 Inductive electromagnetic coupling. Another possible explanation is related to the inductive electromagnetic coupling between the measuring cables and injection cables (e.g. Routh & Oldenburg 2001), which can be responsible for the existence of secondary electrical fields that may affect the measured values, particularly in the intermediate frequency range. According to Volkmann & Klitzsch (2015), 2 electrodes set-up are more suitable to perform SIP measurement at frequencies above 1 kHz because they reduce the EM coupling magnitude between the cables. To assess for the magnitude of these instrumental effects in this case, we performed measurements on pure resistors, for which the theoretical magnitude of the phase measured is 0 on the whole frequency spectrum, since electronic resistors are pure ohmic materials. Measurements were realized on a range of resistors going from 30 to 660 Ohm, which corresponds to the resistance range measured during the different experiments. A detailed description of this study is given in Kremer *et al*. (2016). To summarize, we identified that non-zero phase values were observable in the intermediate frequency range, testifying of the existence of instrumental effects, and that their magnitude increases with frequency and with the resistance value. However, we showed that these instrumental effects cause variations that are always 1 or 2 orders of magnitude lower than the measured values, indicating that the influence of instrumental effects and EM coupling is negligible, which is not surprising since the measuring cables are shielded and well separated from the sample and the injection cables.

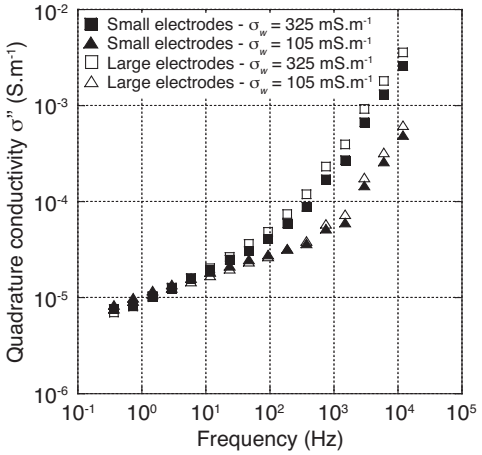

Figure 7. Quadrature conductivity values measured with small and large non polarizable electrodes, on silica sand fully saturated with water of two different conductivities.

6.2.2.4 Influence of the electrodes. As non-polarizable electrode were used for data acquisition, we disregard the hypothesis proposed by Smith-Rose (1934), Keller & Licastro (1959) or Howell & Licastro (1961) that high permittivity values result from electrode polarization effects. However, non-polarizable electrodes can still have a non-negligible effect on the SIP response of Earth materials, because they generally exhibit high contact impedance values. Those effects start being non-negligible for frequencies above 1 kHz, that is in the intermediate frequency range (Huisman *et al*. 2016), and their magnitude increases with contact impedance value (Abdulsamad *et al*. 2014).

A preliminary study was performed to assess whether variations of the electrodes contact impedance could have an effect on the measured quadrature conductivity values in the intermediate frequency range. Two sets of non-polarizable electrodes of different length, and hence of different volumes and different intrinsic impedances were designed. Fig. 7 shows the quadrature conductivity values measured with the two different sets of electrodes on silica sands fully saturated with water of two different EC values. Towards the intermediate frequency range, the quadrature conductivity values increase

with the electrode size and hence with the electrode impedance value. The observed difference is not very large compared to the effect of varying water EC value, but this is not very surprising considering the fact that changing the electrode length only affect slightly the electrode impedance value, since the electrode design remains globally the same (same diameter, same fluid composition, etc.). However, these preliminary results show that the electrode impedance value might indeed have a non-negligible effect on the intermediate frequency response of our studied media, and suggest that the use high impedance of non-polarizable electrodes can be regarded as a viable hypothesis to explain the high permittivity behaviour observed in this study.

This observation means that the absolute SIP response of Earth material in the intermediate frequency range cannot be known unless the electrode contribution to the signal is fully determined. However, if one uses the same set of electrode on different materials or on a media whose physico-chemical properties are evolving with time, the signal variations in the intermediate frequency range can be related to petro-physical parameters or to physical modifications of the studied media.

7 CONCLUSIONS

The SIP response of sands fully saturated with water of several EC values has been modelled using a flexible mechanistic and empirical approach. In the low frequency range (0.5–100 Hz), the quadrature conductivity spectra is modelled using the TLM model from Leroy *et al*. (2008) by adjusting some parameters by trials and errors. In the intermediate frequency range (10^2–10^5 Hz) the calibration is obtained by assigning relatively high relative dielectric permittivity values (to the medium for the empirical approach or to the sand particle for the mechanistic approach). A linear relationship has been identified between the modelled dielectric values and the bulk conductivity of the studied media.

The origin of the dispersion behaviour in this frequency range could be of different nature. Current knowledge on the subject and additional measurements suggest that the high impedance of the non-polarizable electrodes or the non-spherical shape of the sand grains could be responsible for this behaviour. It is possible that these effects occur simultaneously, although more experimental and modelling work needs to be achieved in order to study quantitatively the contribution of each effect.

ACKNOWLEDGEMENTS

We gratefully acknowledge the support of the CO2 research program co-funded by ADEME, TOTAL and SCHLUMBERGER and their permission to publish this paper. However, the views expressed here are those of the authors who are solely responsible for any errors. We address special thanks to A. Gendrin, J. Desroches, and M. Carney (SCHLUMBERGER) for their useful suggestions, as well as to Dr A. Ghorbani for letting us use the Matlab code implementing the grain polarization model. We also thank the reviewers and the editor for their helpful comments. This is IPGP contribution n°3774.

REFERENCES

Abdulsamad, F., Florsch, N., Schmutz, M. & Camerlynck, C., 2014. The paradox of the measuring electrodes in IP, in *Proceedings of the 3rd International Workshop on Induced Polarization*, pp. 48–49, eds Camerlynck, C., Chauris, H., Maineult, A. & Schmutz, M., 6–9 April 2014, Oléron Island, France.

Abdulsamad, F., Florsch, N., Schmutz, M. & Camerlynck, C., 2016. Assessing the high frequency behavior of non-polarizable electrodes for spectral induced polarization measurements, *J. appl. Geophys.,* in press, doi:10.1016/j.jappgeo.2016.01.001.

Arcone, S.A. & Boitnott, G.E., 2012. Maxwell–Wagner relaxation in common minerals and a desert soil at low water contents, *J. Appl. Geophys.,* **81,** 97–105.

Bairlein, K., Hördt, A. & Nordsiek, S., 2014. The influence on sample preparation on spectral induced polarization of unconsolidated sediments, *Near Surf. Geophys.,* **12,** 667–677.

Binley, A., 2015. R3t version 1.8 Software and User Guide.

Binley, A., Slater, L.D., Fukes, M. & Cassiani, G., 2005. Relationship between spectral induced polarization and hydraulic properties of saturated and unsaturated sandstone, *Water Resour. Res.,* **41,** W12417, doi:10.1029/2005WR004202.

Binley, A., Hubbard, S.S., Huisman, J.A., Revil, A., Robinson, D.A., Singha, K. & Slater, L.D., 2015. The emergence of hydrogeophysics for improved understanding of subsurface processes over multiple scales, *Water Resour. Res.,* **51,** 3837–3866.

Breede, K., Kemna, A., Esser, O., Zimmermann, E., Vereecken, H. & Huisman, J.A., 2012. Spectral induced polarization measurements on variably saturated sand–clay mixtures, *Near Surf. Geophys.,* **10,** 479–489.

Bruggeman, V.D., 1935. Berechnung verschiedener physikalischer Konstanten von heterogenen Substanzen. I. Dielektrizitätskonstanten und Leitfähigkeiten der Mischkörper aus isotropen Substanzen, *Ann. Phys.,* **416,** 636–664.

Bücker, M. & Hördt, A., 2013. Analytical modelling of membrane polarization with explicit parametrization of pore radii and the electrical double layer, *Geophys. J. Int.,* **194,** 804–813.

Chelidze, T. & Guéguen, Y., 1999. Electrical spectroscopy of porous rocks: a review—I. Theoretical models, *Geophys. J. Int.,* **137,** 1–15.

Chelidze, T., Guéguen, Y. & Ruffet, C., 1999. Electrical spectroscopy of porous rocks: a review—II. Experimental results and interpretation, *Geophys. J. Int.,* **137,** 16–34.

Chen, Y. & Or, D., 2006. Effects of Maxwell–Wagner polarization on soil complex dielectric permittivity under variable temperature and electrical conductivity, *Water Resour. Res.,* **42,** W06424, doi:10.1029/2005WR004590.

Chew, W.C. & Sen, P.N., 1982. Dielectric enhancement due to electrochemical double layer: thin double layer approximation, *J. Chem. Phys.,* **77,** 4683–4693.

Clavaud, J.-B., 2001. Etude des propriétés de transport (hydraulique et électrique) des roches. Effets de la microstructure, de la présence de plusieurs fluides, de la fracturation et de l'intéraction eau-roche, *PhD thesis,* Université Paris-Diderot.

Cole, K.S. & Cole, R.H., 1941. Dispersion and absorption in dielectrics I. Alternating current characteristics, *J. Chem. Phys.,* **9,** 341–351.

Cosenza, P., Camerlynck, C. & Tabbagh, A., 2003. Differential effective medium schemes for investigating the relationship between high-frequency relative dielectric permittivity and water content of soils, *Water Resour. Res.,* **39,** 1230, doi:10.1029/2002WR001774.

Cosenza, P. & Tabbagh, A., 2004. Electromagnetic determination of clay water content: role of the microporosity, *Appl. Clay Sci.,* **26,** 21–36.

Davidson, D.W. & Cole, R.H., 1951. Dielectric relaxation in glycerol, propylene glycol and n-propanol, *J. Chem. Phys.,* **19,** 1484–1490.

De Lima, O.A. & Sharma, M.M., 1990. A grain conductivity approach to shaly sandstones, *Geophysics,* **55,** 1347–1356.

Dias, C.A., 2000. Developments in a model to describe low-frequency electrical polarization of rocks, *Geophysics,* **65,** 437–451.

Gabriel, S., Lau, R.W. & Gabriel, C., 1996. The dielectric properties of biological tissues: II. Measurements in the frequency range 10 Hz to 20 GHz. *Phys. Med. Biol.,* **41,** 2251–2269.

Garrouch, A.A. & Sharma, M.M., 1994. The influence of clay content, salinity, stress, and wettability on the dielectric properties of brine-saturated rocks: 10 Hz to 10 MHz, *Geophysics,* **59,** 909–917.

Gomaa, M.M., 2008. Relation between electric properties and water saturation for hematitic sandstone with frequency, *Ann. Geophys.,* **51,** 801–811.

Guichet, X., Jouniaux, L. & Catel, N., 2006. Modification of streaming potential by precipitation of calcite in a sand-water system: laboratory measurements in the pH range from 4 to 12, *Geophys. J. Int.,* **166,** 445–460.

Hanai, T., 1968. Electrical properties of emulsions, in *Emulsion Science*, pp. 354–477. ed. Sherman, P., Academic Press.

Hilhorst, M.A., 2000. A pore water conductivity sensor, *Soil Sci. Soc. Am. J.,* **64,** 1922–1925.

Howell, B.F. & Licastro, P.H., 1961. Dielectric behavior of rocks and minerals, *Am. Mineral.,* **46,** 269–288.

Hubbard, S.S., Peterson, J.E., Jr, Majer, E.L., Zawislanski, P.T., Williams, K.H., Roberts, J. & Wobber, F., 1997. Estimation of permeable pathways and water content using tomographic radar data, *Leading Edge,* **16,** 1623–1630.

Huisman, J.A., Zimmermann, E., Esser, O., Haegel, F.-H., Treichel, A. & Vereecken, H., 2016. Evaluation of a novel correction procedure to remove electrode impedance effects from broadband SIP measurements, *J. appl. Geophys.,* in press, doi:10.1016/j.jappgeo.2015.11.008.

Ishai, P.B., Talary, M.S., Caduff, A., Levy, E. & Feldman, Y., 2013. Electrode polarization in dielectric measurements: a review, *Meas. Sci. Technol.,* **24,** 102001, doi:10.1088/0957-0233/24/10/102001.

Jones, S.B. & Friedman, S.P., 2000. Particle shape effects on the effective permittivity of anisotropic or isotropic media consisting of aligned or randomly oriented ellipsoidal particles, *Water Resour. Res.,* **36,** 2821–2833.

Jougnot, D., Ghorbani, A., Revil, A., Leroy, P. & Cosenza, P., 2010. Spectral induced polarization of partially saturated clay-rocks: a mechanistic approach, *Geophys. J. Int.,* **180,** 210–224.

Keller, G.V. & Licastro, P.H., 1959. *Dielectric Constant and Electrical Resistivity of Natural-State Cores,* US Government Printing Office.

Kenyon, W.E., 1984. Texture effects on megahertz dielectric properties of calcite rock samples, *J. appl. Phys.,* **55,** 3153–3159.

Knight, R.J. & Nur, A., 1987. The dielectric constant of sandstones, 60 kHz to 4 MHz, *Geophysics,* **52,** 644–654.

Kremer, T., Schmutz, M., Maineult, A. & Agrinier, P., 2016. Laboratory monitoring of CO_2 injection in saturated silica and carbonated sands using spectral induced polarization, in press, doi:10.1093/gji/ggw333.

Lasne, Y., Paillou, P., Freeman, A., Farr, T., McDonald, K.C., Ruffié, G. & Demontoux, F., 2008. Effect of salinity on the dielectric properties of geological materials: implication for soil moisture detection by means of radar remote sensing, *Geosci. Remote Sens. IEEE Trans.,* **46,** 1674–1688.

Leroy, P. & Revil, A., 2009. A mechanistic model for the spectral induced polarization of clay materials, *J. geophys. Res.,* **114**(B10), B10202, doi:10.1029/2008JB006114.

Leroy, P., Devau, N., Revil, A. & Bizi, M., 2013. Influence of surface conductivity on the apparent zeta potential of amorphous silica nanoparticles, *J. Colloid Interface Sci.,* **410,** 81–93.

Leroy, P., Revil, A., Kemna, A., Cosenza, P. & Ghorbani, A., 2008. Complex conductivity of water-saturated packs of glass beads, *J. Colloid Interface Sci.,* **321,** 103–117.

Lesmes, D.P. & Frye, K.M., 2001. Influence of pore fluid chemistry on the complex conductivity and induced polarization responses of Berea sandstone, *J. geophys. Res.,* **106**(B3), 4079–4090.

Lesmes, D.P. & Morgan, F.D., 2001. Dielectric spectroscopy of sedimentary rocks, *J. geophys. Res.,* **106,** 13 329–13 346.

Maxwell, J.C., 1892. *A Treatise on Electricity and Magnetism,* 3rd edn, Oxford Clarendon Press.

Mendelson, K.S. & Cohen, M.H., 1982. The effect of grain anisotropy on the electrical properties of sedimentary rocks, *Geophysics,* **47,** 257–263.

Olhoeft, G., 1985. Low-frequency electrical properties, *Geophysics,* **50,** 2492–2503.

Persson, M., 2002. Evaluating the linear dielectric constant-electrical conductivity model using time-domain reflectometry, *Hydrol. Sci. J.,* **47,** 269–277.

Pride, S., 1994. Governing equations for the coupled electromagnetics and acoustics of porous media, *Phys. Rev. B,* **50,** 15 678–15 696.

Radic, T., 2004. Elimination of cable effects while multi-channel SIP measurements, in *Near Surface 2004 – 10th European Meeting of Environmental and Engineering Geophysics,* Utrecht, The Netherlands.

Radic, T., 2014. Measuring IP effects at high frequencies: first lab and field data from 0.001 Hz–250 kHz, in *Proceedings of the 3rd International Workshop on Induced Polarization,* pp. 74–75, eds Camerlynck, C., Chauris, H., Maineult, A. & Schmutz, M. 6–9 April 2014, Oléron Island, France.

Revil, A., 2000. Thermal conductivity of unconsolidated sediments with geophysical applications, *J. geophys. Res.,* **105**(B7), 16 749–16 768.

Revil, A., 2013. Effective conductivity and permittivity of unsaturated porous materials in the frequency range 1 mHz–1 GHz, *Water Resour. Res.,* **49,** 306–327.

Revil, A. & Glover, P.W.J., 1998. Nature of surface electrical conductivity in natural sands, sandstones, and clays, *Geophys. Res. Lett.,* **25,** 691–694.

Revil, A., Karaoulis, M., Johnson, T. & Kemna, A., 2012. Review: some low-frequency electrical methods for subsurface, *Hydrogeol. J.,* **20,** 617–658.

Routh, P.S. & Oldenburg, D.W., 2001. Electromagnetic coupling in frequency-domain induced polarization data: a method for removal, *Geophys. J. Int.,* **145,** 59–76.

Scott, J.H., Carroll, R.D. & Cunningham, D.R., 1967. Dielectric constant and electrical conductivity measurements of moist rock: a new laboratory method, *J. geophys. Res.,* **72,** 5101–5115.

Sen, P.N., 1981. Relation of certain geometrical features to the dielectric anomaly of rocks, *Geophysics,* **46,** 1714–1720.

Sen, P.N. & Chew, W.C., 1983. The frequency dependent dielectric and conductivity response of sedimentary rocks, *J. Microwave Power,* **18,** 95–105.

Sengwa, R.J. & Soni, A., 2006. Low-frequency dielectric dispersion and microwave dielectric properties of dry and water-saturated limestones of Jodhpur region, *Geophysics,* **71,** G269–G277.

Smith-Rose, R.L., 1934. Electrical measurements on soil with alternating currents, *J. Inst. Electr. Eng.,* **75**(452), 221–237.

Sze, S.M. & Ng, K.K., 2006. *Physics of Semiconductor Devices,* John Wiley & Sons.

Tabbagh, A., Panissod, C., Guérin, R. & Cosenza, P., 2002. Numerical modeling of the role of water and clay content in soils' and rocks' bulk electrical conductivity, *J. geophys. Res.,* **107,** ECV 20-1–ECV 20-9.

Tabbagh, A., Cosenza, P., Ghorbani, A., Guérin, R. & Florsch, N., 2009. Modelling of Maxwell–Wagner induced polarisation amplitude for clayey materials, *J. appl. Geophys.,* **67,** 109–113.

Taherian, M.R., Kenyon, W.E. & Safinya, K.A., 1990. Measurement of dielectric response of water-saturated rocks, *Geophysics,* **55,** 1530–1541.

Topp, G.C. & Reynolds, W.D., 1998. Time domain reflectometry: a seminal technique for measuring mass and energy in soil, *Soil Tillage Res*., **47,** 125–132.

Vaudelet, P., Revil, A., Schmutz, M., Franceschi, M. & Bégassat, P., 2011. Induced polarization signatures of cations exhibiting differential sorption behaviors in saturated sands, *Water Resour. Res.,* **47,** W02526, doi:10.1029/2010WR009310.

Vinegar, H. & Waxman, M., 1984. Induced polarization of shaly sands, *Geophysics,* **49,** 1267–1287.

Volkmann, J. & Klitzsch, N., 2015. Wideband impedance spectroscopy from 1 mHz to 10 MHz by combination of four-and two-electrode methods. *J. appl. Geophys.,* **114,** 191–201.

Wagner, K.W., 1914. Erklärung der dielektrischen Nachwirkungsvorgänge auf Grund maxwellscher Vorstellungen, *Electr. Eng.,* **2,** 371–387.

Weller, A., Slater, L., Nordsiek, S. & Ntarlagiannis, D., 2010. On the estimation of specific surface per unit pore volume from induced polarization: a robust empirical relation fits multiple data sets, *Geophysics,* **75,** WA105–WA112.

West, L.J., Handley, K., Huang, Y. & Pokar, M., 2003. Radar frequency dielectric dispersion in sandstone: implications for determination of moisture and clay content, *Water Resour. Res.,* **39,** 1026, doi:10.1029/2001WR000923.

Wu, Y., Versteeg, R., Slater, L. & LaBrecque, D., 2009. Calcite precipitation dominates the electrical signatures of zero valent iron columns under simulated field conditions, *J. Contam. Hydrol.,* **106,** 131–143.

Zimmermann, E., Kemna, A., Berwix, J., Glaas, W., Münch, H.M. & Huisman, J.A., 2008. A high-accuracy impedance spectrometer for measuring sediments with low polarizability, *Meas. Sci. Technol.,* **19,** 105603, doi:10.1088/0957-0233/19/10/105603.